

# Three-dimensional colloidal interference lithography

Hironori Nagai, Austen Poteet, Xu A Zhang and Chih-Hao Chang

Department of Mechanical and Aerospace Engineering, North Carolina State University, Raleigh, NC 27695, United States of America

E-mail: [chichang@ncsu.edu](mailto:chichang@ncsu.edu)

Received 9 December 2016, revised 20 January 2017

Accepted for publication 3 February 2017

Published 23 February 2017



CrossMark

## Abstract

Light interactions with colloidal particles can generate a variety of complex three-dimensional (3D) intensity patterns, which can be utilized for nanolithography. The study of particle–light interactions can add more types of intensity patterns by manipulating key factors. Here we investigate a novel 3D nanolithography technique using colloidal particles under two-beam coherent illuminations. The fabricated 3D nanostructures are hollow, nested within periodic structures, and possess multiple chamber geometry. The effects of incident angles and particle size on the fabricated nanostructures were examined. The relative phase shift between particle position and interference pattern is identified as another significant parameter influencing the resultant nanostructures. A numerical model has been developed to show the evolution of nanostructure geometry with phase shifts, and experimental studies confirm the simulation results. Through the introduction of single colloidal particles, the fabrication capability of Lloyd’s mirror interference can now be extended to fabrication of 3D nanostructure with complex shell geometry. The fabricated hollow nanostructures with grating background could find potential applications in the area of photonics, drug delivery, and nanofluidics.

Keywords: nanolithography, three-dimensional nanostructures, colloids, self-assembly, interference lithography

(Some figures may appear in colour only in the online journal)

## Introduction

Three-dimensional (3D) nanostructures have found many interesting applications in the area of photonics and plasmonics [1–5], energy [6, 7], drug delivery [8–13], and others. For certain applications, different types of nanostructures are usually needed. For example, drug delivery applications require hollow nanostructures while photonic applications need periodic nanostructures. Therefore, a large variety of fabrication techniques have been developed, and they can be generally categorized as ‘top-down’ and ‘bottom-up’ techniques. ‘Top-down’ techniques, such as electron-beam lithography [14], two-photon polymerization [15–18], and focused ion beam milling [19], usually require complex hardware systems. Although complex 3D nanostructures can be fabricated using these techniques, throughput is relatively low and process can be costly. In ‘bottom-up’ techniques, colloidal particle self-

assembly can serve as a representative technique with characteristics of low cost and high throughput, and is promising for scaled-up manufacturing. Colloidal particles can act as building elements and be assembled into 3D nanostructures such as opal structures [20]. In addition, colloidal particle arrays have been used as physical masks for metal-assisted chemical etching and focusing element for laser ablation [21–23]. However, the presence of defects and the low variety of assembly architectures are limiting factors in colloidal particle self-assembly. Recently, there has been progress in roll-to-roll coating of colloidal particle assemblies with the potential to scale up 3D nanostructure fabrication [24].

The combination of ‘top-down’ and ‘bottom-up’ techniques takes advantage of both techniques, and has enabled more complex nanostructures. In our previous work [25–27], colloidal particle assemblies were employed as optical phase masks for 3D nanolithography. For example, regular colloidal

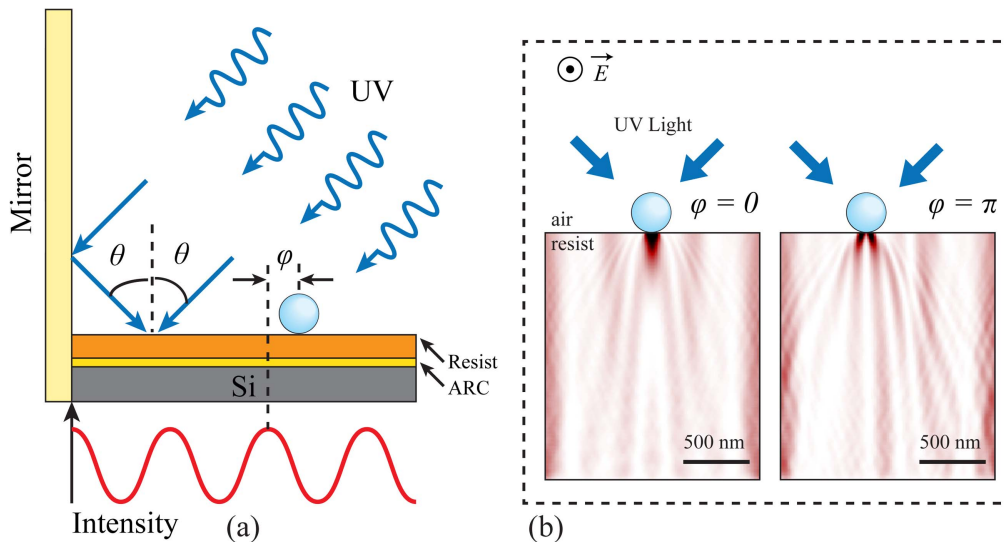


**Figure 1.** (a) Fabrication process of colloidal interference lithography. (b) FDTD simulation showing a cross section of the 3D intensity pattern produced by TE-polarized UV light and a single nanosphere for 0 and  $\pi$  phase shifts. Red and white indicate high and low intensities, respectively.

particle assemblies modulate particle–light interactions and can produce periodic 3D light distributions by Talbot effects [25]. Mie scattering of single isolated particles can also be harnessed to produce normal and oblique ‘nano-volcanoes’ [26, 27]. In addition, 3D nanostructures with complex symmetries were achieved using sequential symmetric multiple exposures. The resultant 3D nanostructures are from the incoherent summation of light scattering intensity from each exposure.

In this work, we investigate the particle–light interactions with coherent two-beam exposures for 3D nanolithography. In this approach, two mutually coherent laser beams are illuminated on an isolated sphere to produce a complex intensity profile. Since the interference pattern of the two incident beams is periodic in one dimension, the relative phase between the fringe pattern and colloidal particle position becomes an added lithography parameter to determine resulting nanostructure geometry, in addition to incidence angle, colloidal particle diameter, and exposure dosage. As a result of the phase difference, the chamber geometry inside the 3D nanostructure can be varied. To model the lithography exposure and predict the fabricated results, a numerical model has been developed using finite-difference time-domain (FDTD) simulation and binary resist model [26, 27]. A Lloyd’s mirror interference lithography system, well known for the fabrication of 1D and 2D periodic nanostructures with high resolution [28, 29], provides the coherent two-beam illuminations. With the incorporation of coherent illuminations, we are able to extend the fabrication capability of colloidal 3D nanolithography.

## Methods

The proposed fabrication process is depicted in figure 1, where a single isolated colloidal particle is illuminated using a

Lloyd’s mirror interference lithography system. In this setup, single ultraviolet (UV) illumination is split into two symmetric, mutually coherent interfering beams. Without the presence of the colloidal particle, a periodic sinusoidal intensity pattern can be generated within the photoresist layer. The presence of colloidal particles on the photoresist surface modulates the light intensity distribution locally through light scattering, as illustrated in figure 1(b) from FDTD simulations. The phase difference between the particle position and the intensity maximum is denoted by  $\varphi$ , which is a key factor in defining resultant 3D nanostructures.

In all experiments, silicon substrates were used to prepare for the samples. A thin layer of photoresist (Sumitomo PFI-88A7) with the thickness of  $1\ \mu\text{m}$  was spin-coated on a silicon wafer to record light intensity pattern. Polystyrene spheres with 1 and  $2\ \mu\text{m}$  diameters (Polysciences, inc. Polybead Microspheres in 2.5% aqueous solution) were spin-coated on photoresist with 1000–2000 rpm for 1 min. The resist sample was dipped in a developer solution (Microposit MF CD-26) and then in deionized water to treat the surface before assembly. The exposures were conducted using a Lloyd’s mirror interference lithography system and a 325 nm wavelength HeCd laser (KIMMON KOHA., ltd) to create the desired coherent condition. The samples were exposed with dosages of  $60\text{--}100\ \text{mJ cm}^{-2}$ , which corresponds to exposure time in the order of 20–30 min. After exposure, the nanospheres were removed by sonication and the photoresist was developed by immersing into developer solution (Microposit MF-CD26) for 2 min. The fabricated samples were characterized using a SEM (JEOL 6400 F) for top and cross section views.

In order to examine the evolution of 3D nanostructures with different phase shifts, the resultant 3D nanostructures can be predicted using FDTD simulation combined with binary resist model [26, 27]. FDTD modeling was performed using the free, open-source software MEEP [30]. To create

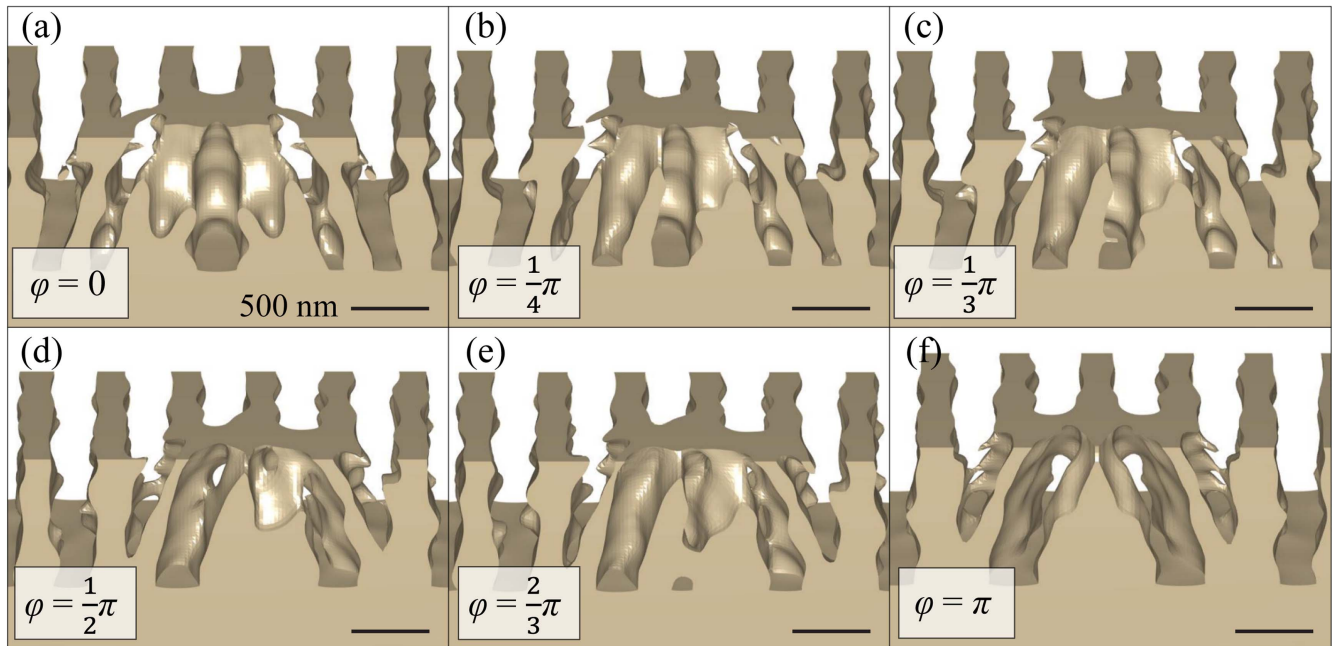


**Figure 2.** 3D nanostructure prediction using FDTD simulation and binary resist model for phase shifts between 0 and  $\pi$ . The particle diameter is  $1 \mu\text{m}$  and the background grating period is  $500 \text{ nm}$  ( $19.0^\circ$  incidence angle).

two oblique incident sources in the simulation, a periodic boundary condition was used to capture the interference between the incident and the reflecting beams. Therefore the simulation domain must be an integer multiple of the period of the interference field pattern, determined by the equation,  $\Lambda = \lambda / \sin(\theta)$ , where  $\Lambda$  is the period,  $\lambda$  is the wavelength, and  $\theta$  is the incident angle. The electric field resulting from the FDTD model was then compared to a threshold value to model a binary photoresist behavior. The intensity values falling above the threshold were removed to model positive photoresist, leaving the resulting structure in 3D space. This 3D structure is represented using Matlab's isosurface and patch functions, which introduce built-in smoothing based on the intensity of the remaining values.

The cross-sectional views of the predicted nanostructures using a positive-tone photoresist for phase shifts from 0 to  $\pi$  are shown in figure 2. This simulation includes  $1 \mu\text{m}$  diameter particle and  $500 \text{ nm}$  grating period, or equivalently,  $19.0^\circ$  incidence angle for two-beam interference. In the background outside of the scattering profile, 1D periodic grating are present as a result of two-beam interference. For figures 2(a)–(f), the grating sidewalls in the vicinity of the colloidal particle are modified and become uneven due to the light scattering field from the colloidal particle. Under the colloidal particle, the coherent summation of the two scattering fields from the two arms of interference generates a complex intensity pattern, resulting in hollow 3D nanostructures. The 3D nanostructures resemble the core–shell ‘nano-volcano’ structures in our previous work, but possess additional features, such as multiple chambers. At zero phase, the three maximum intensity lobes from focusing effects and interference pattern are combined to form a single large chamber. As the phase shift increases, the chamber geometry gradually transforms into two separate chambers until  $\pi$  phase shift,

where the interference pattern reaches zero intensity, and the focusing effect is still present to form two separate chambers. The observations from simulations will be verified by experiments, as discussed in the next section.

## Results and discussion

The proposed fabrication method takes advantages of the scattering intensity pattern produced by transverse electric (TE)-polarized UV light and a single nanosphere. In figure 3, top and cross-section scanning electron microscope (SEM) images of the fabricated 3D nanostructures are illustrated with various combinations of particle diameters and laser incident angles. In these experiments, the significant parameters are diameters of particles and period, which can be controlled by the laser incident angles. Linearly polarized laser with  $325 \text{ nm}$  wavelength was utilized to illuminate the particles. In figures 3(a)–(c),  $500 \text{ nm}$  period and  $1 \mu\text{m}$  diameter particles were used, and the laser incident angle was  $19.0^\circ$ . The top view in figure 3(a) shows two chambers that are created by two laser beams; it also depicts the  $\pi$  phase shift between particle and the background grating lines caused by the interference fringes. The cross-section views of the fabricated double-chamber structures are shown in figures 3(b) and (c) with orthogonal cutting directions. The double-chamber geometry is clearly illustrated with a central separation core, which is caused by only the focusing effect of the nanosphere. The double-chamber geometry is also observed in the predicted structures in figure 2 under  $\pi$  phase shift. More complicated structures can be fabricated using  $2 \mu\text{m}$  diameter particles with  $2 \mu\text{m}$  period and the laser incident angle of  $4.7^\circ$ , as shown in figures 3(d)–(e). Different alignments with grating lines are observed with different resulting structures.

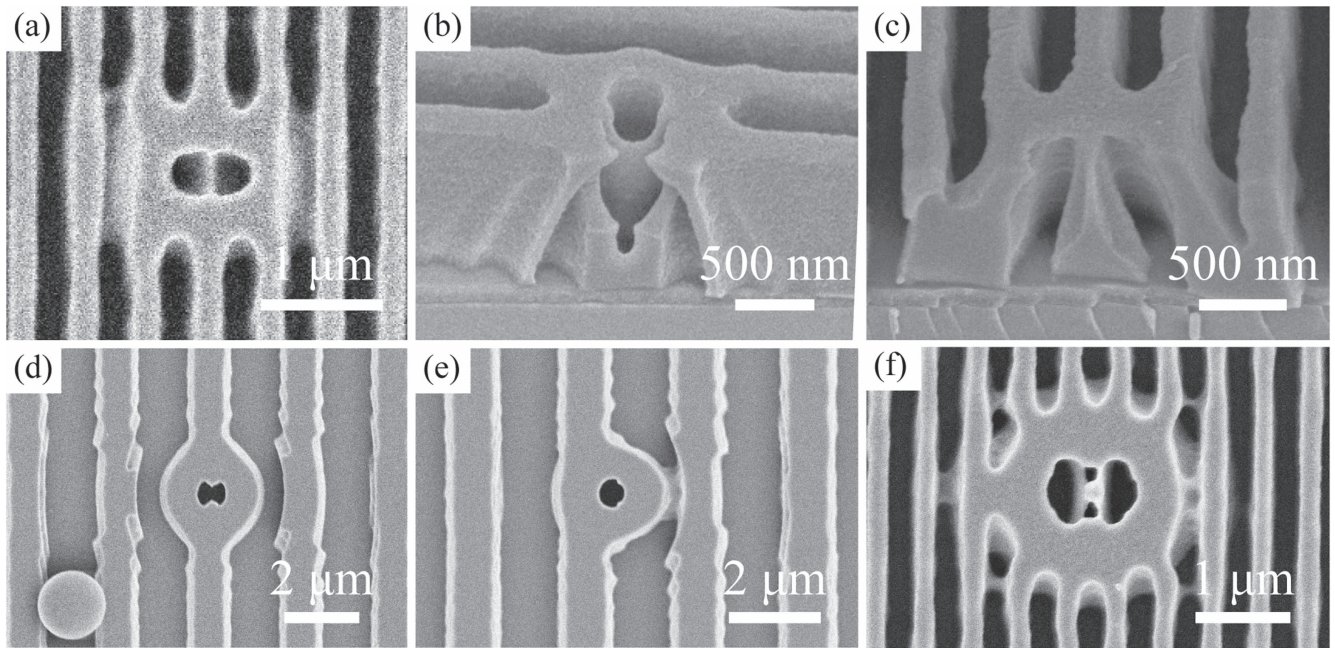


**Figure 3.** Scanning electron micrographs of the fabricated 3D nanostructures with (a)–(c) 500 nm period and 1  $\mu\text{m}$  diameter, (d)–(e) 2  $\mu\text{m}$  period and 2  $\mu\text{m}$  diameter, (f) 500 nm period and 2  $\mu\text{m}$  diameter.

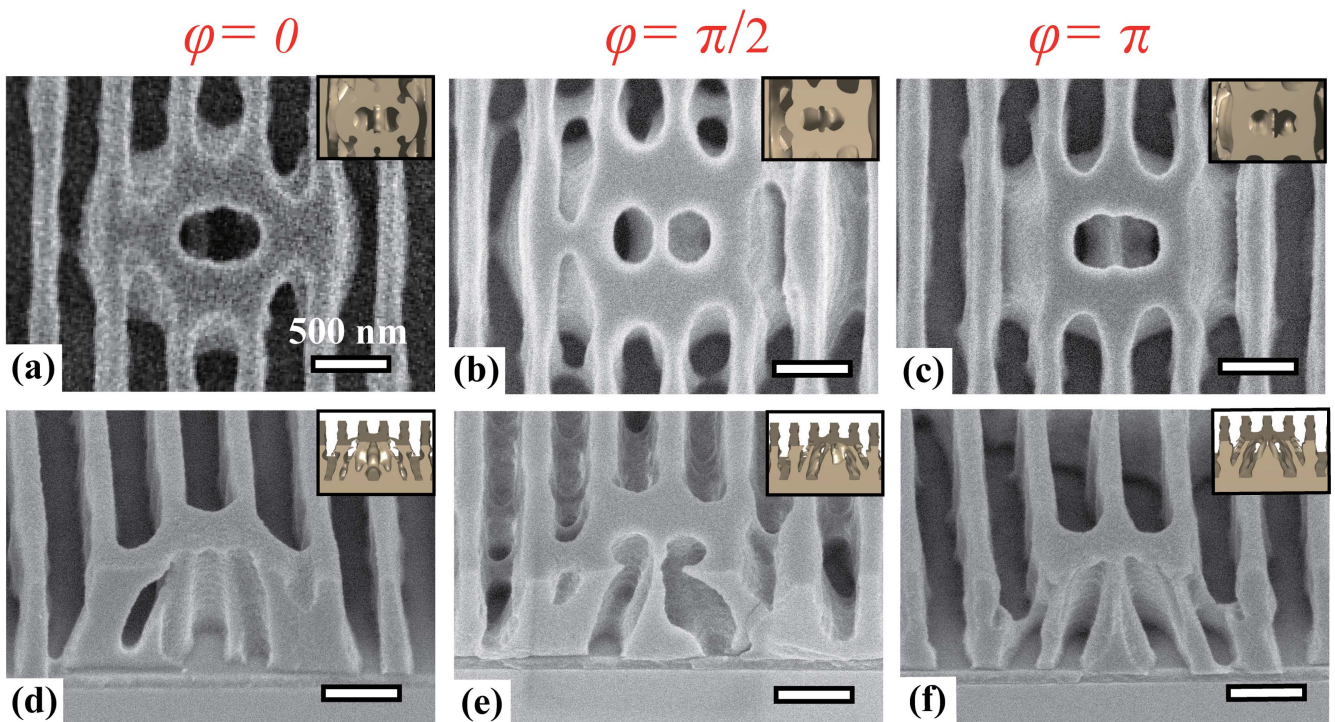


**Figure 4.** Scanning electron micrographs of the fabricated nanostructures with 0,  $\pi/2$ , and  $\pi$  phase shifts. Top (a)–(c) and cross section views (d)–(f) of the fabricated nanostructures with 500 nm period and 1  $\mu\text{m}$  diameter spheres. The insets are predicted nanostructures using FDTD simulation and binary resist model.

Due to the larger particle size, the light scattering pattern can influence larger areas and causes wavy features around the chambers. Different shapes of structures can be achieved by simply increasing the laser incident angle, as illustrated when comparing figures 3(d)–(e) with figure 3(f). By changing the particle size and incident angle, various types of nanostructures can be demonstrated using this fabrication method.

While the fabricated structures are isolated, regular arrays can be potentially fabricated using an array of isolated particles generated through plasma etching of close-packed colloidal assemblies [26].

There are some design constraints to consider when selecting particle diameter, illumination wavelength, and grating period. Since Mie scattering yields the most

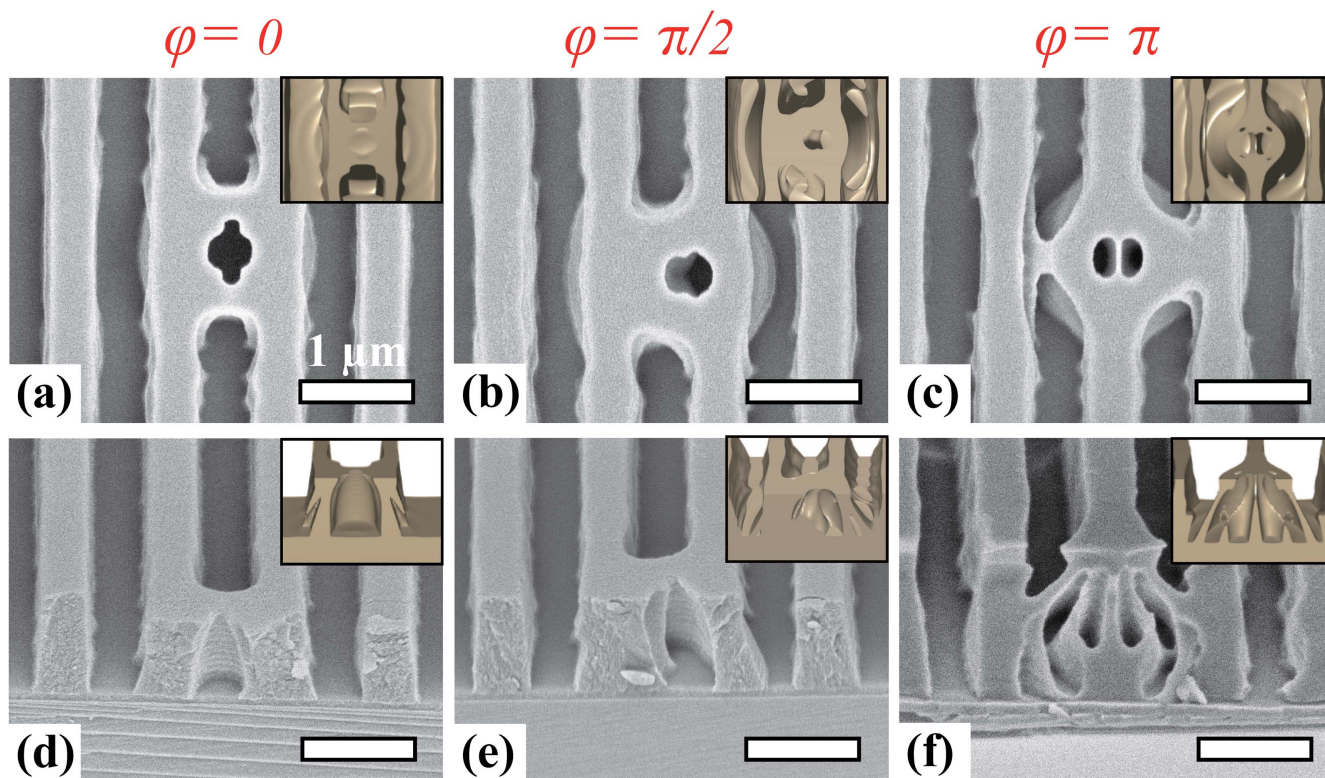


**Figure 5.** Scanning electron micrographs of the fabricated nanostructures with 0,  $\pi/2$ , and  $\pi$  phase shifts. Top (a)–(c) and cross section views (d)–(f) of the fabricated nanostructures with 1  $\mu\text{m}$  period and 1  $\mu\text{m}$  diameter spheres. The insets are predicted nanostructures using FDTD simulation and binary resist model.

interesting angular intensity patterns [26], the particle is typically selected to be similar or slightly larger than the exposure wavelength. Smaller particles will result in shell-like geometries, as shown in figures 3(a)–(c), while larger particles will result in disk-like geometry, as illustrated in figures 3(d)–(f). The grating period, which depends on illumination wavelength and incident angle, can then be selected independently to incorporate the structure. Further experiments were focused on 500 nm and 1  $\mu\text{m}$  grating period with 1  $\mu\text{m}$  diameter nanosphere to examine the phase shift dependence of the nanostructures.

Based on the location of nanosphere under interference lithography, different phase shift patterns can be achieved such as under phase shifts of 0,  $\pi/2$  and  $\pi$ , as shown in figure 4. The SEM images show both top views (a), (b), and (c) and cross-section views (d), (e), and (f) of the 3D nanostructures with phase shifts of 0,  $\pi/2$  and  $\pi$ , respectively. The inset diagrams in figure 4 show the simulated structures. Figures 4(a) and (d) show only one chamber that is created by two laser beams. Because the laser intensity is the highest with zero phase shift, the intensity under the nanosphere is focused, matching well with figure 2(a). In figures 4(b) and (e), two unsymmetrical chambers were observed because the intensity patterns under the nanosphere are not evenly balanced with  $\pi/2$  phase shift. In another case, two symmetric chambers were observed with  $\pi$  phase shift in figures 4(c) and (f). A separation core is observed in the middle of the structure that isolates two symmetric chambers as a result of destructive interference.

Figure 5 shows the fabrication results of 1  $\mu\text{m}$  diameter spheres and 1  $\mu\text{m}$  period, with the incident angle of  $9.4^\circ$  and phase shifts of 0,  $\pi/2$ , and  $\pi$ . Similar changes in structures due to phase shift were expected to be observed; however, different shapes of structures are fabricated due to the larger period. Since the laser incident angle is smaller than the previous experiment, the width of the scattering intensity patterns under nanosphere is narrower as well. In figure 5(a), there is one hollow chamber without any complex structures. For  $\pi/2$  phase shift, separate chamber cannot be observed. With  $\pi$  phase shift sample shown in figure 5(f), multiple chambers and core-shell structures can be generated by using smaller laser incident angle. In smaller laser incident angles, the light intensity distribution resembles the normal incidence case in our previous work, and produce core-shell hollow 3D nanostructures.

## Conclusion

In this work, 3D colloidal interference lithography under coherent two-beam exposure is proposed, and different shapes of 3D nanostructures can be fabricated with various laser incident angles, particle diameters, and phase shifts. FDTD simulation and binary resist model are used to predict the fabricated 3D nanostructures, and provide guidance on the evolution of nanostructures with phase shifts. The scattering intensity under the nanosphere, which can be controlled by changing the phase shifts, has a significant contribution to the

different nanostructures, as demonstrated by our experimental results. The proposed colloidal interference lithography technique can create both symmetrical and unsymmetrical nanostructures with multiple chambers. In addition to phase shifts, the shapes of chambers can also be controlled by laser incident angle and nanosphere diameter. Future work will focus on methods to precisely and uniformly control the nanosphere position in an ordered array to achieve desired phase shifts and yield different types of structures over large areas. The fabricated double-chamber nanostructures could find potential applications in photonics, drug delivery, and nanofluidics.

## Acknowledgments

This work was performed in part at the NCSU Nanofabrication Facility (NNF) and the Analytical Instrumentation Facility (AIF), members of the North Carolina Research Triangle Nanotechnology Network (RTNN), which is supported by the National Science Foundation (Grant ECCS-1542015) as part of the National Nanotechnology Coordinated Infrastructure (NNCI). This work was supported by a NASA Office of the Chief Technologist's Space Technology Research Opportunity—Early Career Faculty grant (grant NNX12AQ46G) and NSF Faculty Early Career Development (CAREER) Program (grant CMMI#1552424).

## References

- [1] Lin S Y *et al* 1998 A three-dimensional photonic crystal operating at infrared wavelengths *Nature* **394** 251–3
- [2] Noda S, Tomoda K, Yamamoto N and Chutinan A 2000 Full three-dimensional photonic bandgap crystals at near-infrared wavelengths *Science* **289** 604–6
- [3] Qi M *et al* 2004 A three-dimensional optical photonic crystal with designed point defects *Nature* **429** 538–42
- [4] De Angelis F *et al* 2013 3D hollow nanostructures as building blocks for multifunctional plasmonics *Nano Lett.* **13** 3553–8
- [5] Ai B, Yu Y, Möhwald H and Zhang G 2013 Responsive monochromatic color display based on nanovolcano arrays *Adv. Opt. Mater.* **1** 724–31
- [6] Fan Z *et al* 2009 Three-dimensional nanopillar-array photovoltaics on low-cost and flexible substrates *Nat. Mater.* **8** 648–53
- [7] Zhang H, Yu X and Braun P V 2011 Three-dimensional bicontinuous ultrafast-charge and -discharge bulk battery electrodes *Nat. Nanotechnol.* **6** 277–81
- [8] (David) Lou X W, Archer L A and Yang Z 2008 Hollow micro-/nanostructures: synthesis and applications *Adv. Mater.* **20** 3987–4019
- [9] Yavuz M S *et al* 2009 Gold nanocages covered by smart polymers for controlled release with near-infrared light *Nat. Mater.* **8** 935–9
- [10] Moon G D *et al* 2011 A new theranostic system based on gold nanocages and phase-change materials with unique features for photoacoustic imaging and controlled release *J. Am. Chem. Soc.* **133** 4762–5
- [11] Peer E, Artzy-Schnirman A, Gepstein L and Sivan U 2012 Hollow nanoneedle array and its utilization for repeated administration of biomolecules to the same cells *ACS Nano* **6** 4940–6
- [12] Prausnitz M R, Mitragotri S and Langer R 2004 Current status and future potential of transdermal drug delivery *Nat. Rev. Drug Discov.* **3** 115–24
- [13] Prausnitz M R and Langer R 2008 Transdermal drug delivery *Nat. Biotechnol.* **26** 1261–8
- [14] Yamazaki K and Yamaguchi H 2008 Three-dimensional alignment with 10 nm order accuracy in electron-beam lithography on rotated sample for three-dimensional nanofabrication *J. Vac. Sci. Technol. B* **26** 2529–33
- [15] Maruo S, Nakamura O and Kawata S 1997 Three-dimensional microfabrication with two-photon-absorbed photopolymerization *Opt. Lett.* **22** 132–4
- [16] Cumpston B H *et al* 1999 Two-photon polymerization initiators for three-dimensional optical data storage and microfabrication *Nature* **398** 51–4
- [17] Kawata S, Sun H-B, Tanaka T and Takada K 2001 Finer features for functional microdevices *Nature* **412** 697–8
- [18] Haske W *et al* 2007 65 nm feature sizes using visible wavelength 3D multiphoton lithography *Opt. Express* **15** 3426–36
- [19] Jeon J, Floresca H C and Kim M J 2010 Fabrication of complex three-dimensional nanostructures using focused ion beam and nanomanipulation *J. Vac. Sci. Technol. B* **28** 549–53
- [20] Gates B, Qin D and Xia Y 1999 Assembly of nanoparticles into opaline structures over large areas *Adv. Mater.* **11** 466–9
- [21] Brodoceanu D, Alhmoud H Z, Elnathan R, Delalat B, Voelcker N H and Kraus T 2016 Fabrication of silicon nanowire arrays by near-field laser ablation and metal-assisted chemical etching *Nanotechnology* **27** 075301
- [22] Choi W K, Liew T H, Dawood M K, Smith H I, Thompson C V and Hong M H 2008 Synthesis of silicon nanowires and nanofin arrays using interference lithography and catalytic etching *Nano Lett.* **8** 3799–802
- [23] Huang Z, Fang H and Zhu J 2007 Fabrication of silicon nanowire arrays with controlled diameter, length, and density *Adv. Mater.* **19** 744–8
- [24] Li X and Gilchrist J F 2016 Large-area nanoparticle films by continuous automated langmuir–blodgett assembly and deposition *Langmuir* **32** 1220–6
- [25] Chang C-H *et al* 2011 From two-dimensional colloidal self-assembly to three-dimensional nanolithography *Nano Lett.* **11** 2533–7
- [26] Zhang X A, Elek J and Chang C-H 2013 Three-dimensional nanolithography using light scattering from colloidal particles *ACS Nano* **7** 6212–8
- [27] Zhang X A, Dai B, Xu Z and Chang C-H 2015 Sculpting asymmetric, hollow-core, three-dimensional nanostructures using colloidal particles *Small* **11** 1285–92
- [28] Smith H I 2001 Low cost nanolithography with nanoaccuracy *Physica E* **11** 104–9
- [29] Bagal A and Chang C-H 2013 Fabrication of subwavelength periodic nanostructures using liquid immersion Lloyd's mirror interference lithography *Opt. Lett.* **38** 2531
- [30] Oskooi A F, Roundy D, Ibanescu M, Bermel P, Joannopoulos J D and Johnson S G 2010 Meep: a flexible free-software package for electromagnetic simulations by the FDTD method *Comput. Phys. Commun.* **181** 687–702